Vertically Aligned CdSe Nanowire Arrays for Energy Harvesting and Piezotronic Devices

Yu Sheng Zhou,[†,∥] Kai Wang,[‡,∥] Weihua Han,[†,§,∥] Satish Chandra Rai,[‡] Yan Zhang,[†] Yong Ding,[†] Caofeng Pan,[†] Fang Zhang,[†] Weilie Zhou,[‡,*] and Zhong Lin Wang[†,⊥,*]

[†]School of Materials Science and Engineering, Georgia Institute of Technology, Atlanta, Georgia 30332-0245, United States, [‡]Advanced Materials Research Institute, University of New Orleans, New Orleans, Louisiana 70148, United States, [§]School of Physical Science and Technology, Lanzhou University, Lanzhou 730000, China, and [⊥]Beijing Institute of Nanoenergy and Nanosystems, Chinese Academy of Sciences, Beijing, China. [∥]These authors contributed equally to this work.

ABSTRACT

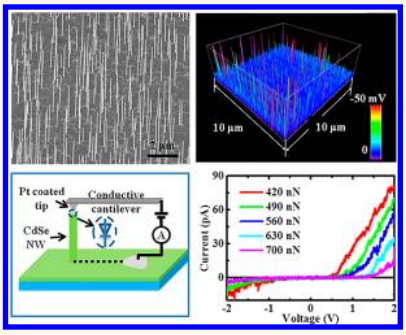

We demonstrated the energy harvesting potential and piezotronic effect in vertically aligned CdSe nanowire (NW) arrays for the first time. The CdSe NW arrays were grown on a mica substrate by the vapor—liquid—solid process using a CdSe thin film as seed layer and platinum as catalyst. High-resolution transmission electron microscopy image and selected area electron diffraction pattern indicate that the CdSe NWs have a wurtzite structure and growth direction along ⟨0001⟩. Using conductive atomic force microscopy (AFM), an average output voltage of 30.7 mV and maximum of 137 mV were obtained. To investigate the effect of strain on electron transport, the current—voltage characteristics of the NWs were studied by positioning an AFM tip on top of an individual NW. By applying normal force/stress on the NW, the Schottky barrier between the Pt and CdSe was found to be elevated due to the piezotronic effect. With the change of strain of 0.12%, a current decreased from 84 to 17 pA at 2 V bias. This paper shows that the vertical CdSe NW array is a potential candidate for future piezo-phototronic devices.

KEYWORDS: CdSe nanowire · piezotronic effect · energy harvesting · piezotronic transistor

Zinc oxide nanomaterials have attracted a lot of interest as building blocks for future nanosystems. Because of its wurtzite structure, a piezoelectric potential (piezopotential) is created in the crystal when stress is applied, due to the polarization of ions along its noncentral symmetric axis. If the piezopotential is used to drive the electron flow through an external circuit, various designs of nanogenerators for self-powered systems can be fabricated.[1−3] Because of its piezoelectric and semiconductor properties, the piezopotential created in the crystal has a strong effect on the carrier transport at the metal—semiconductor interface. Piezotronic devices use the piezopotential as a "gate" voltage to tune/control the charge carrier transport at a contact or junction.[4−8] Furthermore, by combining the semiconductor photonic excitation and transition properties, it has been proven that the piezopotential can be used to control the carrier generation, transport, separation, and/or recombination in what is called the piezo-phototronic effect. This has been used to improve the performance of optoelectronic devices,[9,10] such as photon detectors,[11] solar cells,[12] and LEDs.[13]

As one of the most important II—VI group semiconductor materials with wurtzite structure, CdSe has been studied extensively in the optoelectronic field. Recently, one-dimensional CdSe nanostructured materials have been reported for potential applications in light-emitting devices,[14] solar cells,[15] photodetectors,[16] and lasers.[17] Combined with its unique optical properties, the CdSe NW is an attractive potential candidate to replace ZnO NWs in hybrid energy harvesting and piezo-phototronic devices. However, little research has been reported on the field on CdSe NWs.

In this paper, we demonstrated the energy harvesting potential and piezotronic effect in CdSe NW arrays for the first time. Vertically aligned CdSe NW arrays with a wurtzite structure were synthesized using the vapor—liquid—solid (VLS) process. By using the conductive AFM in contact mode, we obtained an average output voltage of 30.7 mV for the CdSe NW arrays. Then by measuring the *I*—*V* characteristics of a single

* Address correspondence to zlwang@gatech.edu, wzhou@uno.edu.

Received for review May 18, 2012 and accepted June 26, 2012.

Published online 10.1021/nn3022074

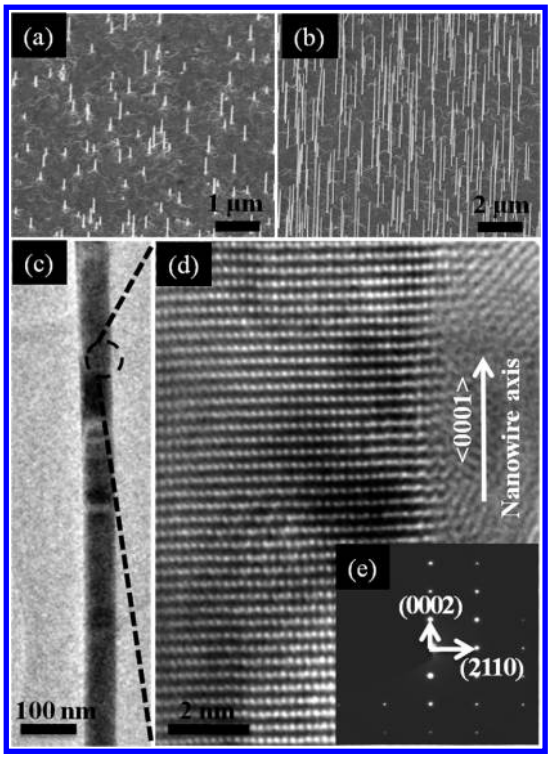

Figure 1. Vertically aligned CdSe NW array grown on the mica substrate. (a) Side-view SEM images of the short (~200−500 nm) NWs and (b) long (~2−4 μm) NWs; (c) TEM image of a NW with low magnification; (d) high-resolution TEM (HRTEM) image of CdSe NW; (e) corresponding selected area electron diffraction (SAED) pattern from the region indicated by the dashed circle in the image.

CdSe NW using a Pt-coated AFM tip, we found that an externally applied force can significantly tune the current through the piezotronic effect. CdSe NW arrays have promising application potentials in the fields of hybrid energy harvesting with solar cells, strain sensors, and piezo-phototronic sensors.

RESULTS AND DISCUSSION

CdSe NWs were grown on mica substrates with CdSe thin film as the seed layer and platinum as the catalyst using VLS. The density and length of the CdSe NWs can be well controlled during the synthesis process. Tilted-view scanning electron microscopy (SEM) images of the as-grown CdSe NWs with different lengths are presented in Figure 1a,b, showing that the length of the NWs varies from 200 nm to 4 μm, but the diameter remains constant. A low-magnification transmission electron microscopy (TEM) image is shown in Figure 1c, and the diameter of the NWs is a uniform 60 nm along the length. The corresponding high-resolution TEM (HRTEM) image and the selected area electron diffraction (SAED) pattern indicate that the CdSe NW has a single crystal wurtzite structure and grows along the ⟨0001⟩ direction, as shown in Figure 1d,e, respectively.

The wurtzite crystal structure of CdSe and simulated piezopotential distribution when the CdSe NW is stressed are shown in Figure 2. The red balls represent

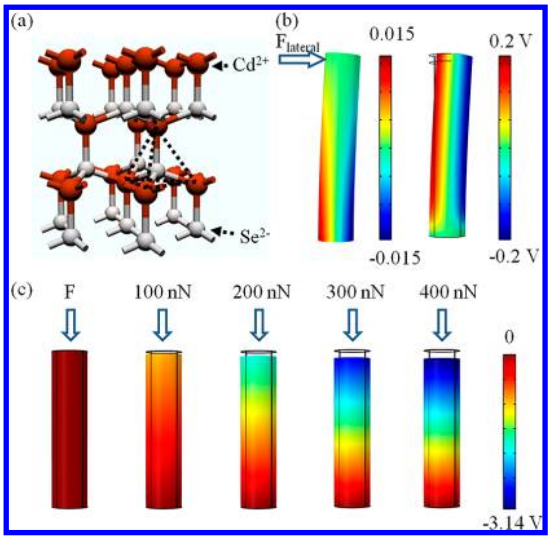

Figure 2. (a) Schematic crystal structure of CdSe NW along ⟨0001⟩ direction; (b) strain and corresponding piezopotential distribution on the surface of NW under a bending force 80 nN in Comsol simulation; (c) piezopotential distribution under normal force ranging from 100 to 400 nN. Geometry of the NW used in the simulation is diameter D = 60 nm and length L = 250 nm.

the Cd^{2+} cations, and the gray balls represent the Se^{2-} anions (Figure 2a). This structure is composed of repeating tetrahedral units, where the Se^{2-} anions are located on the corners while the Cd^{2+} cations are in the center. The positive and negative charge centers overlap under strain-free conditions. Once a stress is applied along the c axis, the charge centers are relatively displaced, resulting in a dipole moment. A macroscopic piezopotential can be created along the NW by adding up all of the dipole moments of the unit cells (Figure 2b,c).

The magnitude of the piezopotential depends on the deformation of the crystal, the doping concentration, and the dielectric constant.[18] Figure 2b,c shows the distribution of the piezopotential along a NW under various forces using the Lippman theory for doping free CdSe NWs. The parameters used for the simulation are shown in Table 1. Figure 2b shows the piezopotential distribution when a lateral force of 80 nN is applied on the upper end of the NW and the other end is fixed and electrically grounded. When the lateral force is applied, the NW is bent and experiences tension on one side and compression on the other side. The tensile side exhibits a positive potential of 202 mV, whereas the compressive side shows a negative potential with the same amplitude. The piezopotential created in such a bent piezoelectric NW can be used to drive the electron flow through an external circuit, making CdSe NWs an electric generator which converts mechanical energy into electrical energy. Under small bending force, the length of the NW has little influence on the piezopotential under a given lateral force. The potential distribution is similar to bent ZnO NW from previous reports,[1] which could be explained by the fact that both of them have the wurtzite structure and c axis along the wire. Figure 2c shows the piezoelectric potential distribution

TABLE 1. Parameters Used for the Simulation of CdSe NW

parameter	value	
length (nm)	250	
diameter (nm)	60	
piezoelectric coupling coefficients matrix (C/m^2)	$e_{31} = -0.16$	
	$e_{33} = 0.347$	
	$e_{15} = -0.138$	
elasticity matrix (GPa)	$C_{12} = 46.1$	$C_{13} = 74.9$
	$C_{15} = 39.3$	$C_{33} = 81.7$
	$C_{44} = 13$	$C_{66} = 14.3$

when the NW is compressed by external normal forces. The top of the NW exhibits a negative potential compared to the bottom. It can be shown that the amplitude of the negative potential increases with increased strain due to further separation of the charges in the crystal cells.

The NW bending mode can be used for energy harvesting with vertically aligned NW arrays, and the vertical compression mode was used to fabricate piezotronic transistors. We demonstrated the potential applications of both modes in CdSe NWs using the following experiments.

Energy Harvesting. The piezoelectric energy harvesting performance of bent CdSe NWs was investigated using a conductive AFM probe. The applied normal force was 140 nN with a scan speed of 40 μm/s. Figure 3a,b shows the topography image and corresponding electric output. The output voltage peak corresponds well to the NWs indicated in the AFM topography image, and about 54% of the NWs had an output. The maximum output voltage was about 137 mV. Figure 3d is a comparison of the topographic profile (red curve) and corresponding voltage output (blue curve) when the tip was scanned from left to right. The negative output was detected when the tip scanned over the NW, indicating that the voltage was detected on the compressive side. This is similar to the previously reported model for n-type ZnO NW.[1]

As illustrated in the inset diagram in Figure 3a, a Schottky contact forms when the Pt-coated AFM tip scans over the NW. When the tip started to bend the NW, the tensile side of the NW had a positive potential, leading to a reversely biased Schottky junction. Thus no current could be detected, and piezoelectric charges accumulated at both sides. When the tip scanned over the NW, the negative potential on the compressive side led the Schottky contact forward biased, driving current flow from the tip to the NW, where a negative signal was detected by the system. This is consistent with previously reported mechanisms.[1] Figure 3e shows the distribution of the output voltage amplitude. Because the length and aspect ratio differ for each NW, the bending force by the AFM tip differs, resulting in a variation in the output voltage. About 40% of the output voltage was between 6 and 12 mV, and another 40% lay in the range from 12 to 42 mV with an average output voltage of 30.7 mV. The current detected ranged from 1 to ~30 pA, which was above the noise level

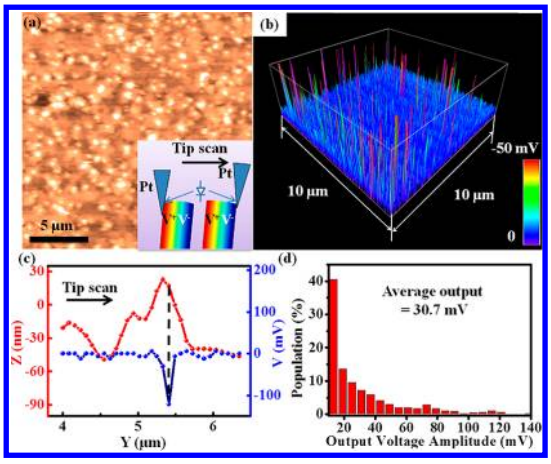

Figure 3. (a) AFM topography of the CdSe NW; the range in *z* direction is 200 nm. The inset is the schematic of the mechanism for collecting the piezoelectric output by AFM tip. (b) Corresponding piezoelectric output voltage shown in the 3D graph. (c) Line profile of topography and piezoelectric output. (d) Statistical distribution of the amplitude of output voltage.

of our system (0.5 pA). The maximum voltage was less than the simulated result, which could be attributed to the fact that the free carriers partially screen the piezopotential in the NW, which was not considered in the simulation.[18]

Piezotronic Effect. By applying a normal force to the top of the CdSe NWs using an AFM tip, the piezotronic effect was investigated. Figure 4a shows the schematic of the experimental setup. Because of the difference between the work function of Pt (6.1 eV)[1] and the electron affinity of CdSe (4.95 eV),[19] a Schottky junction forms between the CdSe NW and Pt-coated tip. The bottom of the NW was connected to a CdSe thin film, to which an electrical contact was made using silver paste. Since the piezoelectric polarization charges only existed at the top surface of the NW and the bottom film surface and the contact between Ag and CdSe film was rather large, the influence of the piezopotential on the bottom Ag−CdSe contact can be neglected. Furthermore, an Ohmic contact was detected by measuring the *I*−*V* characteristics of a Ag−CdSe−Ag structure, which is probably due to the work function of Ag (4.26 eV)[1] being lower than the electron affinity of CdSe. Therefore, it is reasonable to assume that the Schottky barrier formed at the Pt−CdSe junction dominates the *I*−*V* characteristics in both directions.

As shown in the aforementioned simulation (Figure 2c), a compressive force applied by the AFM tip would induce a negative piezopotential in the CdSe. This piezopotential would change the local Schottky barrier height (SBH) through internal field, as illustrated by energy band diagram in Figure 4b. The larger the force applied, the more the barrier increases.

Figure 4c shows the experimental results of the *I*−*V* measurement under increasing applied forces, starting at 420 nN. In the beginning, the reverse current was very small while the forward current started to increase from bias of 0.5 V and reached 84 pA at a bias voltage of 2 V, indicating a current rectifying phenomenon. As the force

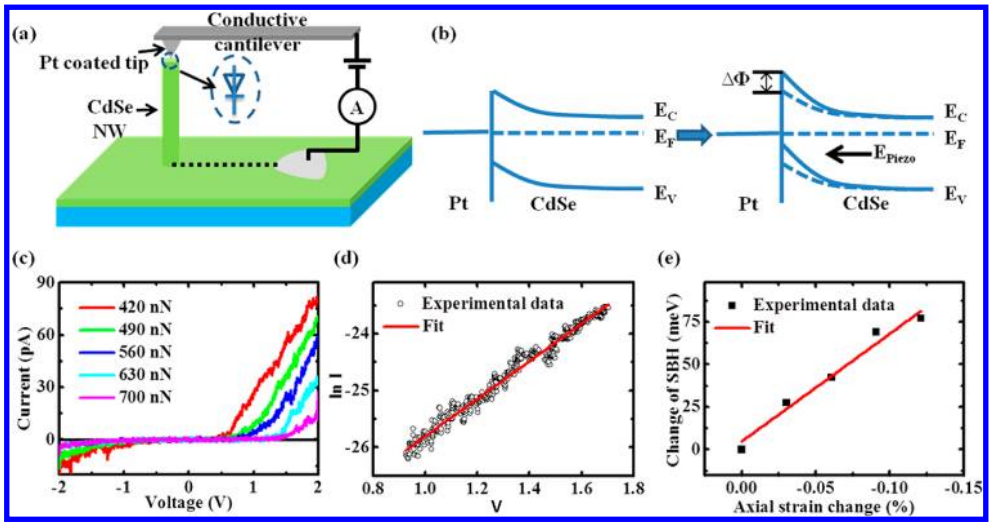

Figure 4. (a) Experimental setup for measuring the piezotronic effect; (b) band diagram of the interface between Pt and CdSe and the change of Schottky barrier by the piezopotential; (c) *I*−*V* characteristics of a single CdSe NW measured by C-AFM under different applied forces; (d) plot of ln *I* as a function of *V*; (e) calculated change in barrier height from the measured *I*−*V* characteristics.

increased to 700 nN in increments of 70 nN, the forward bias decreased dramatically to 17 pA at a bias of 2 V.

To evaluate the influence of the applied axial strain on the Schottky barrier of the CdSe NW, we calculated the SBH change according to the *I*−*V* characteristics.[4,5] For the sake of simplicity, we assume an ideal Schottky diode by neglecting the shunt and series resistance and apply the thermionic current−voltage relationship described by eq 1:[20]

$$I_f = AA^{**}T^2\exp\left(-\frac{\phi_B}{k_BT}\right)\exp\left(\frac{qV_f}{nk_BT}-1\right) \quad (1)$$

where A is the area of the Schottky barrier, A^{**} is the effective Richardson constant, T is the temperature, Φ_B is the SBH, k_B is the Boltzmann constant, q is the electron charge, V_f is the voltage drop on the forward biased Schottky diode, and n is the ideality factor.

To verify that eq 1 could precisely describe the observed *I*−*V* characteristic, we plot ln *I* as a function of *V*, as given in Figure 4d. In this figure, the ln *I*−*V* curve fairly linear, which indicates that the thermionic emission−diffusion model is the dominant process in this experiment and the model could be applied to derive the SBH change from the *I*−*V* characteristics. Therefore, assuming that the change of A^{**} under strain is much smaller than the strain-induced change in the SBH,[5] we can calculate the change of the SBH by

$$\ln(I_f(\varepsilon_1)/I_f(\varepsilon_2)) \sim -\Delta\phi_s/kT \quad (2)$$

As shown in Figure 4e, the SBH changes linearly with increased axial strain of the CdSe NW. The barrier height increased by 77.1 meV with strain change of 0.12%. The variation of the SBH could be mainly attributed to a combination of the piezoresistive and piezotronic effect.[4] The piezoresistive effect is a change in resistance of a semiconductor due to a change in band gap and local carrier density and is symmetrical. This effect will modulate the current symmetrically at both the forward and reverse bias. For the piezotronic effect, the change of SBH induced will lead the current changing asymmetrically due to its polarity. According to previous reported theoretical and experimental mechanisms,[5,10,21] this stress-induced asymmetric current modulation is mainly attributed to the piezotronic effect.

CONCLUSION

In summary, we reported the growth of vertically aligned CdSe NW arrays and investigated their energy harvesting and piezotronic effect by AFM for the first time. The energy harvesting performance of CdSe NW arrays is comparable with that of previously reported ZnO NW arrays. By applying the normal force on the top of the CdSe NWs via the AFM tip, the Schottky barrier height between Pt and CdSe NW was modulated and resulted in a current decrease from 84 to 17 pA with a 0.12% difference in strain at 2 V bias. This phenomenon was mainly attributed to the piezotronic effect. On the basis of the piezoelectric and piezotronic properties investigated in this paper, combined with the reported optical properties, CdSe NW arrays have promising application potentials in the hybrid energy harvesting with solar cell, strain sensor, and piezo-phototronic sensor areas.

EXPERIMENTAL METHODS

Synthesis of Vertically Aligned CdSe NW Arrays. The vertically aligned CdSe NW arrays were grown by thermal evaporation on muscovite mica substrates with CdSe thin films and platinum particles as the barrier and catalysts, respectively. First, freshly cleaved muscovite mica substrates (SPI, grade V-5 research quality)

were loaded into an electron beam evaporation system (Kurt J. Lesker, PVD75) for CdSe thin film deposition. After being coated with 100 nm CdSe thin film, the mica substrates were transferred to sputtering system (Cressington coating system, 308R) for platinum catalyst deposition. The nominal thickness of the catalyst was 0.3 nm. CdSe powder (Alfa Aesar, 99.999% purity, metal basis) loaded in the molybdenum crucible was used as the evaporation material source. The growth was carried out in a typical thermal evaporation horizontal tube furnace where the mica substrate was placed downstream to collect the products. The furnace was then heated to 750 °C with H_2/Ar flow (30 sccm/120 sccm) to generate vapor for 20 min. The samples were taken out for characterizations after the system was cooled to room temperature.

Morphology and Structure Characterization. Morphological and crystallographic characterization was performed by using a LEO 1530 field emission scanning electron microscope (FE-SEM) system and a JEOL-4000 transmission electron microscope (TEM).

Electrical Measurements with Conductive Atomic Force Microscope (C-AFM). The characterization of the piezoelectric and piezotronic effect was achieved by using a MFP-3D AFM system from Asylum Research. The probes used in the scans were AC-240TM from Olympus with a Ti(5 nm)/Pt(20 nm)-coated tip. The thermal noise method was employed to determine the spring constant of the cantilever probes. The applied force was estimated as the product of probe spring constant, inverse optical lever sensitivity (InvOLS), and cantilever deflection (represented by voltage). During NG characterization, the deflection set point was kept at 840 mV. The output current was detected by the preamplifier in the AFM system, and output voltage was calculated as the product of measured output current and the resistance of the substrate. In the piezotronic measurement, the AFM tip was positioned on top of one CdSe NW and the electrical measurements were carried out. The magnitude of the force was kept constant by keeping the deflection set point during one measurement.

Conflict of Interest: The authors declare no competing financial interest.

Acknowledgment. This research was supported by BES, DOE, MURI from the Air Force, MANA NIMS, and the Air Force. The authors would like to thank Dr. Cheng-Ying Chen, Dr. Ya Yang, Dr. Lin Dong, Ruomeng Yu, and Ken C. Pradel for their helpful discussions.

REFERENCES AND NOTES

1. Wang, Z. L.; Song, J. H. Piezoelectric Nanogenerators Based on Zinc Oxide Nanowire Arrays. *Science* **2006**, *312*, 242–246.
2. Pan, C. F.; Li, Z. T.; Guo, W. X.; Zhu, J.; Wang, Z. L. Fiber-Based Hybrid Nanogenerators for/as Self-Powered Systems in Biological Liquid. *Angew. Chem., Int. Ed.* **2011**, *50*, 11192–11196.
3. Xu, S.; Qin, Y.; Xu, C.; Wei, Y. G.; Yang, R. S.; Wang, Z. L. Self-Powered Nanowire Devices. *Nat. Nanotechnol.* **2010**, *5*, 366–373.
4. Zhou, J.; Gu, Y. D.; Fei, P.; Mai, W. J.; Gao, Y. F.; Yang, R. S.; Bao, G.; Wang, Z. L. Flexible Piezotronic Strain Sensor. *Nano Lett.* **2008**, *8*, 3035–3040.
5. Zhou, J.; Fei, P.; Gu, Y. D.; Mai, W. J.; Gao, Y. F.; Yang, R.; Bao, G.; Wang, Z. L. Piezoelectric-Potential-Controlled Polarity-Reversible Schottky Diodes and Switches of ZnO Wires. *Nano Lett.* **2008**, *8*, 3973–3977.
6. Wu, W. Z.; Wei, Y. G.; Wang, Z. L. Strain-Gated Piezotronic Logic Nanodevices. *Adv. Mater.* **2010**, *22*, 4711–4715.
7. Han, W. H.; Zhou, Y. S.; Zhang, Y.; Chen, C. Y.; Lin, L.; Wang, X.; Wang, S. H.; Wang, Z. L. Strain-Gated Piezotronic Transistors Based on Vertical Zinc Oxide Nanowires. *ACS Nano* **2012**, *6*, 3760–3766.
8. Ku, N. J.; Huang, J. H.; Wang, C. H.; Fang, H. C.; Liu, C. P. Crystal Face-Dependent Nanopiezotronics of an Obliquely Aligned InN Nanorod Array. *Nano Lett.* **2012**, *12*, 562–568.
9. Wang, Z. L. Progress in Piezotronics and Piezo-Phototronics. *Adv. Mater.* **2012**, 10.1002/adma.201104365.
10. Wang, Z. L. Piezopotential Gated Nanowire Devices: Piezotronics and Piezo-Phototronics. *Nano Today* **2010**, *5*, 540–552.
11. Yang, Q.; Guo, X.; Wang, W. H.; Zhang, Y.; Xu, S.; Lien, D. H.; Wang, Z. L. Enhancing Sensitivity of a Single ZnO Micro-/Nanowire Photodetector by Piezo-Phototronic Effect. *ACS Nano* **2010**, *4*, 6285–6291.
12. Zhang, Y.; Yang, Y.; Wang, Z. L. Piezo-Phototronics Effect on Nano/Microwire Solar Cells. *Energy Environ. Sci.* **2012**, *5*, 6850–6856.
13. Yang, Q.; Wang, W. H.; Xu, S.; Wang, Z. L. Enhancing Light Emission of ZnO Microwire-Based Diodes by Piezo-Phototronic Effect. *Nano Lett.* **2011**, *11*, 4012–4017.
14. Colvin, V. L.; Schlamp, M. C.; Alivisatos, A. P. Light-Emitting-Diodes Made from Cadmium Selenide Nanocrystals and a Semiconducting Polymer. *Nature* **1994**, *370*, 354–357.
15. Yu, Y. H.; Kamat, P. V.; Kuno, M. A CdSe Nanowire/Quantum Dot Hybrid Architecture for Improving Solar Cell Performance. *Adv. Funct. Mater.* **2010**, *20*, 1464–1472.
16. Jiang, Y.; Zhang, W. J.; Jie, J. S.; Meng, X. M.; Fan, X.; Lee, S. T. Photoresponse Properties of CdSe Single-Nanoribbon Photodetectors. *Adv. Funct. Mater.* **2007**, *17*, 1795–1800.
17. Li, G. H.; Zhai, T. Y.; Jiang, Y.; Bando, Y.; Golberg, D. Enhanced Field-Emission and Red Lasing of Ordered CdSe Nanowire Branched Arrays. *J. Phys. Chem. C* **2011**, *115*, 9740–9745.
18. Gao, Y.; Wang, Z. L. Equilibrium Potential of Free Charge Carriers in a Bent Piezoelectric Semiconductive Nanowire. *Nano Lett.* **2009**, *9*, 1103–1110.
19. Swank, R. K. Surface Properties of 2−6 Compounds. *Phys. Rev.* **1967**, *153*, 844.
20. Schroder, D. K. *Semiconductor Material and Device Characterization*, 3rd ed.; Wiley: New York, 2006; p xv, 779pp.
21. Zhang, Y.; Liu, Y.; Wang, Z. L. Fundamental Theory of Piezotronics. *Adv. Mater.* **2011**, *23*, 3004–3013.